6

Submitted "Composites A"

Nano-Scale Characterisation of Interphase In Silane Treated Glass Fibre Composites

Jang-Kyo KIM, Man-Lung SHAM and Jingshen WU
Department of Mechanical Engineering,
Hong Kong University of Science & Technology,
Clear Water Bay, Kowloon, Hong Kong

Abstract

The properties of the interphase formed between glass fibre with differing silane coupling agents and a vinylester resin are characterised using novel experimental techniques, including nanoindentation and nanoscratch tests and thermal capacity jump measurement. The effective interphase thickness measured from the nanoscratch test varies between 0.8μm and 1.6μm depending on the type and concentration of silane agent. These values are consistent with those measured based on the heat capacity changes, in terms of both general trend and absolute quantity. They increase with increasing silane concentration, as expected. The nanoindentation test is not sensitive enough to distinguish the difference in interphase thickness due to different silane agents, while it gave the interphase thickness approximately 1μm, with some varying elastic modulus and hardness values for the matrix resin.

Keywords: Interphase thickness; glass fibre-vinylester composite; nanoindentation test; nanoscratch test; thermal capacity measurement.

1. Introduction

A bond between fibre and polymer matrix materials may be formed by the interdiffusion of atoms or molecules across the interface through a thermodynamic equilibrium between the two constituents. The interphase formed thereby possesses chemical, physical and mechanical properties that are different from those of either bulk fibre or matrix acting alone. In brief, the interphase presents a transition region of which properties vary continuously between the fibre and the matrix. The interphase may have a substantial thickness depending on the molecular conformation, the constituents involved, the ease of molecular motion, and most importantly, whether or not the fibres are treated with polymeric sizes and/or other coupling agents [1]. Epoxy and vinylester matrix composites reinforced with glass fibres have been the major driving force in the development of composites technology for the past three decades, partly indebted to the benefits of silane coupling agents. Silane agents that are applied to glass fibre surfaces as a size along with other components are designed to protect the glass fibre surfaces and act as a coupling agent to promote the adhesion with the polymer matrix. Several theories have been proposed to explain the interface adhesion mechanisms that are responsible for the improvement of mechanical performance and hygrothermal stability of composites containing silane treated glass fibres. Among these, the chemical bonding mechanism is the most important mechanical/physiochemical phenomena. However, an optimal mechanical strength cannot be achieved only through the chemical bonding of silane agents with the composite constituents. An established view is that bonding through silane other than chemical reactivity is best explained by interdiffusion and the formation of an interpenetrating network (IPN) at the interphase region [2-4].

The interphase region created thereby is complicated by the number of components and the interactions that occur between the silane and glass fibre surface. It is suggested that the

polymeric and lubricant components of size dissolve into the surrounding resin and that the silane migrate to the fibre surface [5]. Whether the interphase material created by interdiffusion of silane sizing is more ductile/brittle and softer/stiffer than the bulk matrix material is an issue of great importance because the interphase properties often dictate the gross mechanical performance of the whole composite. Although a great deal of research has been directed toward characterization of the interphase properties, including modulus, ductility and size, there still exist no consensus. This is due primarily to the experimental difficulties involved and lack of appropriate techniques required for accurate measurements of the properties. In polymer matrix composites, the interphase is found to be significantly softer than the bulk matrix material [6-8]. For example, the high spatial resolution measurement of elastic displacements suggested that the carbon fibre-epoxy matrix interphase had a modulus one quarter of that of the bulk matrix [7]. However, the effective modulus of the interphase in close vicinity of the fibre as measured from indentation tests [6,7,9] was known to be even greater than that of the bulk matrix, due to the presence of a stiff fibre that would mitigate the effect of a soft interphase. The postulation of a softer interphase than the bulk matrix discussed above is supported by the lower apparent fibre pull-out bond strength obtained for the silane treated glass fibre-polyester system [10]. The thick layer of γ-methacryloxypropyltrimethylsilane (MPS) applied on glass fibres plasticized the inherently brittle polyester resin, rendering the interphase material softer than the bulk matrix. On the contrary, almost completely reversed observation was reported [11]. The mechanical properties of the blend of silane/size and bulk epoxy resin (at concentrations representing likely compositions found at the fibre-matrix interface region) tended to have a lower glass transition temperature, T_g, higher modulus and tensile strength and lower fracture toughness than the bulk matrix. The monotonic decrease in T_g with increasing size content, suggests that the silane and other size ingredients reduced the crosslink density of mixtures. It was

postulated [7] that even without the size on fibres, the cross-link density of the interphase is lower than the bulk matrix, because the amine present in the resin tends to be adsorbed onto the fibre surface [12]. This appears to rather contradict to the earlier finding that the crosslink density tended to be higher nearer the glass fibre surface, due to the migration of silane migrate onto to the fibre surface during the curing process [13]. The composites fabricated with treated fibres showed a higher interlaminar shear strength (ILSS), and flexural strength than the composite without size treatment. Higher strengths were obtained in both the longitudinal and transverse directions, solid evidence of improved interface adhesion due to the silane coupling agent [11].

Apart from the mechanical properties of interphase relative to the bulk matrix material, the effective thickness or width of interphase has also been of particular interest. Polarised optical microscopy has been widely employed to identify the transcrystallised interphase surrounding isolated fibres in semi-crystalline thermoplastic composites, see for example [14,15]. For thermoset matrix composites, several novel techniques have been devised to study the interphase with varying degree of success. They include the nanoindentation [6,7,16], atomic force microscopy (AFM) [17] and scanning force microscopy (SFM) with indentation [12]. The thickness of interphase region in a carbon/epoxy composite was estimated to be approximately 0.5μm based on the nanoindentation technique [7]. The AFM in force modulation mode was successfully employed to visualize interphase of 1 to 3μm in thickness for sized carbon/epoxy and glass/polypropylene (PP) systems [17]. The unsized fibres had an interphase region that was too small for characterization using the SFM whose lateral resolution being even greater than the interphase thickness [12,18]. In addition to the foregoing techniques, a great number of experimental methods, many based on spectroscopy [2-5], have been successfully used to characterise the effective thickness of interphase.

The present study is a continuation of our on-going project on evaluation of the mechanical properties of glass woven fabric composites affected by silane coupling agent. To select optimum interfacial conditions that would provide balanced mechanical properties and fracture resistance, a series of mechanical test have been carried out in our previous work [19-22]. In this study, an attempt is made to characterize the properties of fibre-matrix interphase affected by different silane agents, based on novel techniques including nano-indentation and nano-scratch tests, and specific heat capacity measurements. Special emphasis was placed on estimation of the effective thickness of interphase.

2. Experimental Procedures

2.1 Materials and Specimens

An E-glass woven fabric reinforced vinylester matrix composites was employed in this study. The reinforcement and the matrix material used and the preparation of composite laminates were essentially the same as those previously reported [19-22]. The glass fabrics were treated with five different coupling agents before being embedded in the matrix material; 0.01wt% (designated as M0.01), 0.4wt% (M0.4), 1.0wt% (M1.0) γ-methacryloxypropyl-trimethoxysilane (γ-MPS); methanol washed 0.4wt% γ-MPS (MW0.4) and 0.4wt% (E0.4) γ-glycidoxypropyltrimethoxysilane (γ-GPS). The nominal diameter of glass fibres was 9μm and the average fibre volume fraction of composite was approximately 42.6% [23]. The major mechanical properties measured previously [23] for the composites with five different silane treatments are summarized in Table 1. For the nanoindentation and nanoscratch tests, composites of 4mm in thickness were cut into small pieces of approximately 10mm x 4mm, which were mounted in a resin mould such that the fibre cross-

sections could be seen on the surface. The surface of the sample was polished using increasingly finer sand papers and was finally finished with aluminium oxide papers of 50nm in particle size. For the specific heat capacity measurements, pieces of neat resin and silane treated composites of 2mm x 2mm square were cut from the plate.

2.2 Nanoindentation and Nanoscratch Tests

All indentation and scratch tests were performed using an indenter (Nanoindenter® II, by Nano Instruments Inc). The indenter consists of an indenter head, an optical microscope connected to a video camera for indentation positioning and a motorized three-dimensional precision table for the transportation of the sample between the microscope and the indenter. A coil-magnet assembly located at the top of the loading column drives the indenter, the displacement is determined by a capacitance displacement gauge. The maximum load capacity of the instrument is over 600mN, and its spatial resolution is 400nm. The indenter head is made up of a three-sided pyramidal diamond with a Berkovich tip, as shown in Figure 1. The length of side wall of the indent is approximately 7.4 times its depth, and the typical tip radius ranges from 50nm to 100nm.

All indentation experiments followed the recommended procedures [24] with multiple loading and unloading along the fibre-interphase-matrix of composite specimen with differing fibre surface treatments. The indenter was programmed such that a series of indents were made 400nm apart, and to a constant indent depth of 60nm, which was equivalent to applied loads of approximately 0.6mN for the glass fibre and less than 0.05mN for the matrix. The indenter depth was though to be shallow enough to prevent any stress field perturbation between adjacent indents.

The hardness, H, and the reduced elastic modulus, E_r, taking into account the effect of non-rigid indenter column, were calculated based on the equations [24,25]:

$$H = \frac{P}{A} = \frac{P}{24.5 h_c^2} \qquad (1)$$

$$E_r = \frac{\sqrt{\pi}}{2\beta}\frac{S}{\sqrt{A}} = \left(\frac{(1-\upsilon_i^2)}{E_i} + \frac{(1-\upsilon_s^2)}{E_s}\right)^{-1} \qquad (2)$$

where P is the maximum load, A is the contact area and h_c is the contact depth of the indent. β is the geometric constant (= 1.034 for a triangular indenter), and S is the unloading stiffness at maximum load. E and ν are the modulus and the Poisson ratio. The subscripts, i and s, refer to the diamond indenter and the specimen, respectively.

The scratch test involved moving the sample while being contact with the indenter tip. The tangential force option of the indenter was employed to measure continuously the indenter depth and the tangential force corresponding to a normal force from the scratch tests. A set of proximity probes and a special scratch test collar were mounted on the original set-up, and the proximity probe measured the lateral deflection of the indenter shaft. The indenter tip was replaced by the scratch tip with the same geometry as the indenter tip, and was oriented with the sharp leading edge being in the scratch direction, as shown in Figure 1 (b). A constant normal force, W = 2.5mN was applied and the tangential (or friction) force, F, was recorded. The tangential force-displacement data were obtained at an interval of approximately 20nm, and the data were analyzed to plot both the depth profile versus scratch length and the coefficient of friction versus scratch length profiles. The coefficient of friction, μ, was calculated based on the following equation:

$$\mu = \frac{F}{W} \qquad (3)$$

At least five scratch tests were conducted for each set of condition. The indented and scratched samples were examined using a scanning electron microscope (SEM).

2.3 Thermal capacity measurement

The effective thickness of interphase was also estimated from the consideration of the differential heat capacity jump between the fibre-reinforced and unfilled reins in the glass transition region [26,27]. This method is based on the principle in that as the reinforcement content or fibre volume fraction is increased, the jump in thermal capacity ΔC in the glass transition region of resin is reduced. It is suggested that the macromolecular state of the polymer resin in the vicinity of rigid reinforcement surface be modified, which is excluded from the process of glass transition [26]. The volume fraction of this modified material (i.e. interphase), λ, is given as:

$$\lambda = 1 - \frac{\Delta C_f}{\Delta C_o} \tag{4}$$

where ΔC_f and ΔC_o are the thermal capacity jumps for the fibre reinforced composite and neat resin, respectively. For a unit thickness of the unidirectional fibre composite schematically shown in Figure 2, the volume fraction ratio of interphase and fibre can be related to the effective thickness of the interphase, t, and λ by:

$$\frac{(t+r_f)^2 - r_f^{\,2}}{r_f^{\,2}} = \frac{(1-V_f)\lambda}{V_f} \tag{5}$$

where r_f and V_f are the fibre radius and the fibre volume fraction, respectively. Rearrangement of equation (5) gives the effective thickness, t:

$$t = r_f\left[\sqrt{1 + \frac{(1-V_f)\lambda}{V_f}} - 1\right] \tag{6}$$

3 Results and Discussion

3.1 Nanoindentation

Typical load-displacement curves and the corresponding SEM photographs of indentations made on the polished cross-section of specimen are shown in Figures 3 and 4, respectively. Because the indent depth was set at a constant value, the indents are shown the same size in Figure 4. Whilst the glass fibre exhibited almost identical loading-unloading paths, the vinylester matrix showed significantly different paths with reversed plasticity upon unloading. The high friction and plastic recovery of the polymer were mainly responsible for the hysteretic loops. See the details of load-displacement curves for the fibre and matrix material obtained at a high load in Figure 5. It was suggested [25] that a sufficient number of loading-unloading cycles be applied to remove the plastic recovery before- accurate measurements of modulus can be made based on the unloading portion of the curve.

The elastic modulus values measured for composites containing different silane agents are plotted along the matrix-interphase-fibre. The modulus of E-glass fibre showed large scattering ranging from 65GPa to 85GPa, with an overall average about 75.5GPa. This value is considered slightly higher than the Young's modulus of 72.4GPa [1]. Meanwhile, the modulus of vinylester varied little, the average being approximately 4.3GPa. A transition region was observed between the fibre and matrix, which had indentation properties and load-displacement curves intermediate between fibre and matrix. The transition region can be regarded as the interphase, which was estimated from the distance between the low and high plateau modulus values in Figure 6. This gave approximately 1μm for all specimens tested. It is clear that the nano-indentation technique was not sensitive enough to measure with reasonable accuracy the effective thickness of interphase that is formed as a result of silane treatment of glass fibre. Distinction between the composites of different surface treatments was difficult because of the limited spatial resolution of the technique arising from the imperfect indenter tip geometry and the certain finite length that should be maintained between adjacent indents to avoid overlapping.

3.2 Nanoscratch Test

Figure 7 presents the variation of tangential force for a constant normal force applied during the scratch test. Plots for typical coefficient of friction and the corresponding penetrating depth profiles are illustrated in Figure 8, while the matching SEM photograph being shown in Figure 9. The vinylester matrix resulted in a higher coefficient of friction and a higher scratch depth than the fibre. The penetrating depth of the tip is a complex function of the normal force applied and the properties, especially the hardness/modulus and wear resistance, of the material being scratched. For a given normal load, the penetrating depth is determined by the contact between the leading edge of scratch tip and the material. There is a transition region between the Points A and B in Figure 8. These points are defined as the intersections of horizontal depth profiles with the two slant lines **a** and **b**, respectively. The thickness of the transition region estimated thereby was 3~4μm, which is considered to be much larger than that obtained from the nano-indentation test. The transition region indeed comprises not only the genuine interphase thickness, but also the region created by the finite width of the indenter tip.

In order to separate the effect of indenter tip geometry, the interactions taking place between the indenter tip and the three composite components during the scratch process were carefully examined and divided into four stages. Figure 10 schematically illustrates the positions of the tip relative to the composite components at different stages of scratch operation. This represents the most common case where the effective thickness of interphase is generally smaller than the penetrating width of the tip. The reversed case is also possible, but was not specifically considered in this study. In Stage I, the scratch tip enters the matrix material and moves toward the interphase. The scratch depth profile remains unchanged until the tip touches the boundary with the interphase. In Stage II, as the scratch tip enters the interphase region, the scratch depth decreases gradually due to the slightly

higher stiffness of the interphase than the matrix material. In general, a low tangential load or a shallow scratch depth reflects a low stiffness of the material. In Stage III, as the scratch tip edge enters the fibre, there is a sudden decrease in scratch depth because of the large changes in stiffness. Scratch to the same depth continues until the tip passes completely out of interphase. The large changes in stiffness between the interphase and fibre are clearly manifested by the two distinct slopes of scratch depth profile, **a** and **b**, as shown in Figure 8. In stage IV, the scratch depth profile becomes flattened once the whole tip moves into the fibre.

Therefore, the net thickness of the interphase was estimated taking into account the scratch tip geometry and the angle between the front edge of the scratch tip and the vertical line perpendicular to the base θ (= 77.3°), see Figure 1. Figure 11 shows the variations of the interphase thickness thereby obtained for different fibre surface treatments. The effective thickness of the interphase varied in the range between 0.8μm and 1.6μm depending on the type and concentration of silane agent. It is highlighted that the thickness increased with increasing the methacryl silane concentration, which is expected. Methanol washing of the silane treated fibre showed marginal increase in interphase thickness, and the composite containing epoxy silane treatment had the smallest interphase thickness amongst composites studied.

3.3 Thermal capacity measurement

Typical thermal capacity-temperature curves for unfilled and reinforced vinyl ester matrix are showed in Figure 12. The extent of thermal capacity jump in the unfilled resin was much higher than those of fibre composites, which is clearly associated with the presence of inactive fibres as well as bound matrix material surrounding the fibre. The effective thicknesses of bound matrix material, i.e. interphase, is calculated based on Equation 4 to 6

and are presented in Figure 13 for different silane treatments. Of note is that the influence of fibre surface treatment on interphase thickness in the heat capacity measurement followed precisely the results obtained from the scratch test in both the qualitative and quantitative terms. The general trend was very much the same between the two methods, with the interphase thickness increasing with increasing the silane concentration. The difference in magnitude was 40% at maximum, with the majority closely matching each other. Only the exception was for the composites with epoxy silane treatment, for which the heat capacity measurement gave much larger interphase thickness than the nano-scratch test. This observation suggests that the former method was more sensitive to a small change in chemical structure within the interphase region than the nanoscratch test. It is postulated that the epoxy silane coupling agent disperses easily into the matrix material during the curing process. The resulting interphase has a gradient property, which can only be fully detected using a sensitive tool, such as heat capacity measurement.

4 Concluding Remarks

Although the concept of interphase in fibre reinforced composites has been widely accepted, very little work has hitherto been made toward direct measurements of interphase thickness. In the present study, novel techniques, including nanoindentation, nanoscratch test and heat capacity measurement, are successfully employed to in-situ measure the effective thickness of interphase region in glass fibre reinforced vinylester matrix composites, and thereby distinguish the different silane agents applied onto the glass fibre. The following conclusions can be highlighted.

i) The nanoindentation test gave the interphase thickness approximately 1μm, although being unable to distinguish different silane agents applied. Nevertheless, it showed varying elastic

modulus and hardness values for the matrix resin, an indication that the bulk resin has been modified to a certain extent by the silane agent.

ii) The effective interphase thickness values measured from the nanoscratch test and based on the heat capacity principle agree well in both the qualitative and quantitative terms. They varied in the range between 0.8μm and 1.6μm depending on the type and concentration of silane agent.

iii) The effective interphase thickness increased with increasing silane concentration, which is consistent with the general perception.

Acknowledgements

The authors wish to thank the Research Grants Council of Hong Kong for continuing support of this project through the grant HKUST817/96E. Most experiments were conducted with the technical supports of Material Characterization & Preparation Facilities (MCPF) and Advanced Engineering Materials Facilities (AEMF) at HKUST.

References

1. J.K. Kim and Y.W. Mai, "Engineered Interfaces in Fiber Reinforced Composites" Elsevier Science, Oxford (1998).

2. E.P. Plueddemann, in "Interfaces in Polymer Matrix Composites", Vol. 6, E.P. Plueddemann (Ed.), Academic Press, New York, (1974).

3. H. Ishida and J.L. Koenig, "An investigation of the coupling agent/matrix interface of fiber glass reinforced plastic by Fourier transform infrared spectroscopic" *J. Polym. Sci. Polym. Phys. Ed.*, **17** (1979) 615-626.

4. H. Ishida and J.L. Koenig, "Effect of hydrolysis and drying on the siloxane bonds of a silane coupling agent deposited on E-glass fibers" *J. Polym. Sci. Polym. Phys. Ed.*, **18** (1980) 233-237.

6. H.C.Tsai, A.M. Arocho & L.W. Gause, "Prediction of fiber-matrix interphase properties and their influence on interface stress, displacement and fracture toughness of composite material" *Mater. Sci. Eng.* **A126** (1990) 295-304.

7. J.G. Williams, M.E. Donnellan, M.R. James & W.L. Morris, "Properties of the interphase in organic matrix composites", *Mat. Sci. & Eng.* **A126** (1990) 305-312.

8. M. Sato, T. Kurauchi & O. Kamigaito, "Relationship between fatigue property and microfailure of interface in composite materials", in *Proc. "Benibana" Intern. Symp. How to Improve the Toughness of Polymers and Composites-Toughness*, Fracture and Fatigue of Polymers and Composites, Yamagata, Japan, 277-284 (1990).

9. A. Garton and J.H. Daly, "Characterisation of the aramid epoxy and carbo-epoxy interphases" *Polym. Composites*, **6** (1985) 195-200.

10. P.S. Chua, S.R. Dai & M.R. Piggott, "Mechanical properties of the glass fibre-polyester interphase" *J. Mater. Sci.*, **27** (1992)913-918.

11. E.K. Drown, H. Al Mouussawi & L.T. Drazl, "Glass fiber 'sizings' and their role in fiber-matrix adhesion", *J. Adhesion Sci. Technol.*, **5**, 865-881 (1991).

12. M.R. van Landingham, R.R. Dagastine, R.F. Eduljee, R.L. McCullogh, J.W. Gillespie Jr, "Characterisation of nanosclae property variations in polymer composite systems, 1. Experimental results" *Composites Part A*, **30A** (1999) 75-83.

13. F.R. Jones, "nterphase formation and control in fibre composite materials" *Key Eng. Mater.* **116-117** (1996) 41-60.

14. J.L. Thomason and A.A. van Rooyen, "Transcrystallised interphase in thermoplastic composites" *J. Mater. Sci.* **27** (1992) 889-896.

15. J.R. Wood, H.D. Wagner and G. Marom, "Transcrystallinity in polycarbonate-carbon fibre microcomposites: the key to the mechanical role of the interphase" *J. Mater. Sci. Lett.* **14** (1995) 1613-1615.

16. H.F. Wang, J.C. Nelson, W.W. Gerberich and H.E. Deve, "Evaluation of in situ mechanical properties of composites by using nanoindentation techniques," *Acta Metall. Mater.* **42** (1994) 695-700.

17. K. Mai, E. Meader and M. Muhle, "Interphase characterization in composites with new non-destructive methods," Composites Part A, **29A** (1998) 1111-1119.

18. T.A. Bogetti, T. Wang, M.R. van Landingham, J.W. Gillespie Jr., "Characterisation of nanosclae property variations in polymer composite systems, 2. Numerical modeling" Composites Part A, **30A** (1999) 85-94.

18. T.A. Bogetti, T. Wang, M.R. van Landingham, J.W. Gillespie Jr., "Characterisation of nanosclae property variations in polymer composite systems, 2. Numerical modeling" Composites Part A, **30A** (1999) 85-94.

19. Y. Hirai, H. Hamada & J.K. Kim, "Impact response of glass woven fabric laminates, Part I. Effect of fibre surface treatment", *Compos. Sci. Technol.*, **58** (1998) 91-104.

20. Y. Hirai, H. Hamada & J.K. Kim, "Impact response of glass woven fabric laminates, Part II. Effect of temperature", *Compos. Sci. Technol.*, **58** (1998) 119-128.

21. M.L. Sham, J.K. Kim & J.S. Wu, "Effects of coupling agent concentration and hygrothermal ageing on the fracture behaviour of glass woven fabric-reinforced vinylester laminates", *Polym. Polym. Composites* **5** (1997)165-175.

22. M.L. Sham, J.K. Kim & J.S. Wu, "Interlaminar properties of glass woven fabric composites: Mode I and Mode II fracture", *Key Eng. Mater.* **145-149** (1998) 799-804.

23. R. Bequignat, P. Krawczak, W. Cantwell, P. Scaramuzzino, M. Desaeger, I. Verpoest, H. Hamada, Y. Hirai, M. Kotaki, M. Hojo, J.K. Kim, J.K. Kocsis, T.J. Mackin, J. Mayer, T. Morii & T. Tanimoto, "Influence of different glass fiber sizings on the mechanical properties of glass fabric composites: Report of a round robin fabric composites: Report of a round robin test," in *Proc. 10th Intern. Conf. On composite materials (ICCM-10)*, Whistler, Canada, Woodhead Publ., Cambridge, UK, 597-603 (1995).

24. W.C. Oliver, G.M. Pharr, "An improved technique for determining hardness and elastic modulus using load and displacement sensing indentation experiments", *J. Mater. Res.* **7** (1992) 1564-1583.

25. S.D. McAdams, T.Y. Tsui, W.C. Oliver & G.M. Pharr, "Effects of interlayers on the scratch adhesion performance of ultra-thin films of copper and gold on silicon substrates", *Mat. Res. Soc. Symp. Proc.* **356** (1995) 809-814.

26. G.C. Papanicolaou, G.J. Messinis & S.S. Katakatsanidis, "The effect of interfacial conditions on the elastic-longitudinal modulus of fibre reinforced composites", *J. Mater. Sci.* **24** (1989) 395-401.

27. R.J. Morgan, "Thermal characterization of composites", in Thermal Characterization of Polymeric Materials", E.A. Turi (Ed.), Academic Press, (1997) Chapter 9.

Figure Captions

Fig. 1 Geometry of Berkovich indentor tip

Fig. 2 Interphase thickness in a unidirectional fibre composite.

Fig. 3 Typical indentation load-displacement curves for fibre, matrix and the transition region.

Fig. 4 SEM microphotographs of a series of indents made along the fibre-interphase and matrix.

Fig. 5 Indentation load-displacement curves of fibre and matrix at a maximum indentation depth of 60nm.

Fig. 6 Variation of elastic modulus across the matrix-interphase-fibre: (a) M0.01; (b) M0.4; (c) M1.0; (d) MW0.4; and (e) E0.4.

Fig. 7 Variations of normal and tangential forces along the matrix-interphase-fibre.

Fig. 8 Profiles of coefficient of friction and scratch depth.

Fig. 9 SEM photograph of scratched surface.

Fig. 10 Schematic illustrations of nanoscratch depth profiles at different stages.

Fig. 11 Variation of effective interphase thickness with silane concentration.

Fig. 12 Typical specific heat capacity curves at glass transition region of unfilled and fibre reinforced vinylester matrix.

Fig. 13 Variations of effective interphase thickness measured from hear capacity jump.

Table 1 Strengths and moduli of glass woven fabric reinforced vinylester matrix composites (± standard deviation).

Type and concentration of silane agent	Strength (MPa)		Modulus (GPa)	
Methacryl silane 0.01wt% (M0.01)	270(21)	372(20)	19.5(5.2)	18.1 (1.5)
0.4wt% (M0.4)	318(16)	431(19)	19.6(5.1)	18.8(1.6)
1.0wt% (M1.0)	329(31)	444(40)	20.2(5.2)	19.7(1.9)
Methanol washed methacryl silane 0.4wt% (M0.4)	338(13)	452(23)	20.4(5.0)	19.4(0.9)
Epoxy silane 0.4wt%	321(32)	380(27)	20.3(5.0)	19.3(1.1)

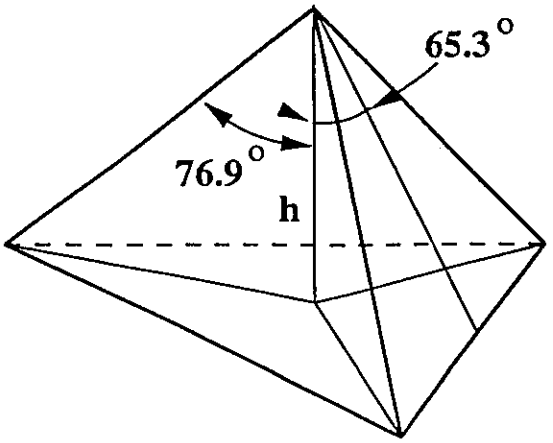

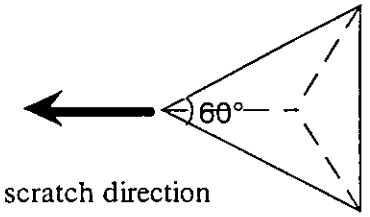

Fig 1

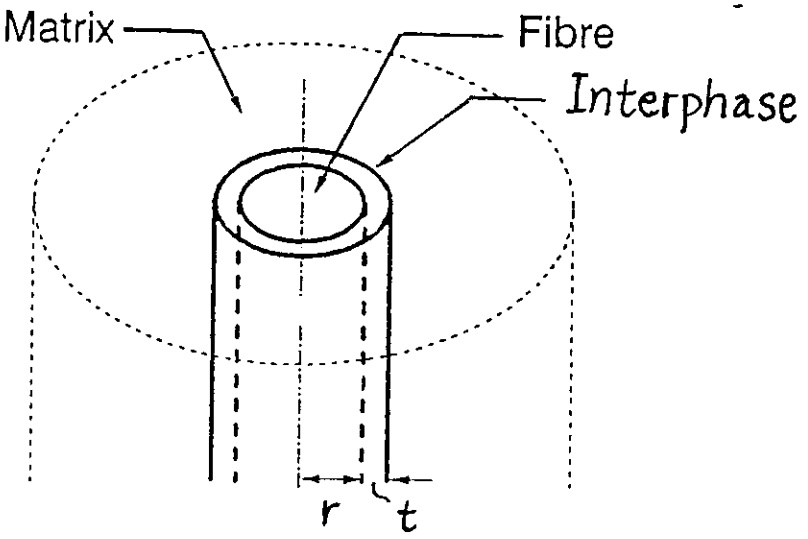

Fig 2

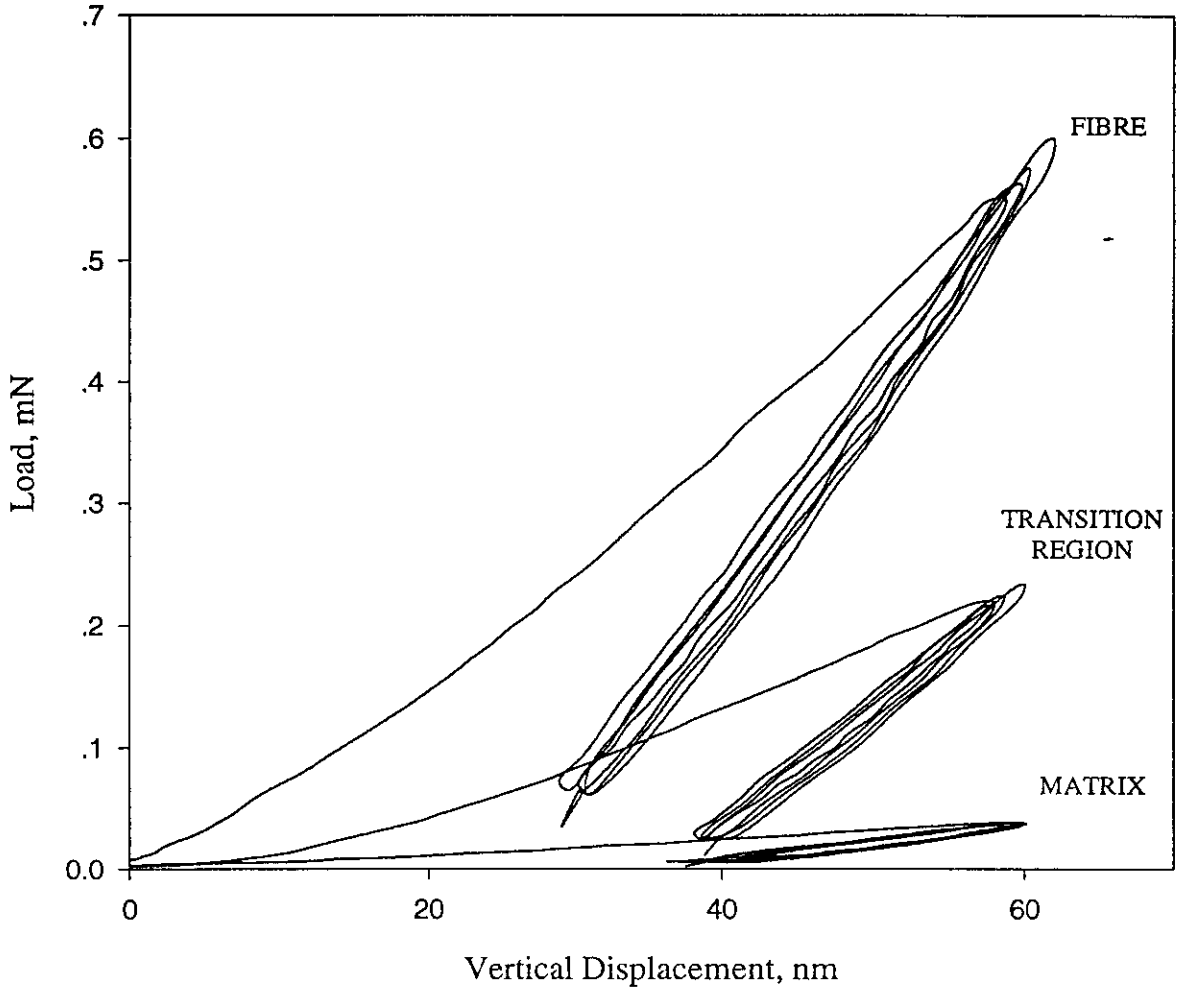
.7
.6
.5
.4
.3
.2
.1
0.0
Load, mN
0
20
40
60
Vertical Displacement, nm
FIBRE
TRANSITION
REGION
MATRIX

Fig 3

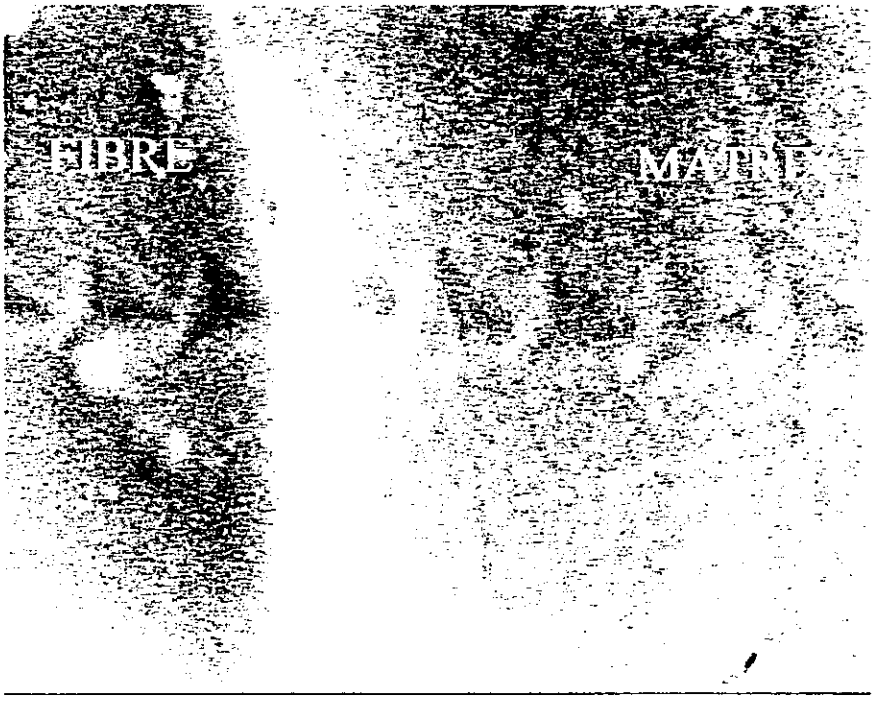

Fig 4

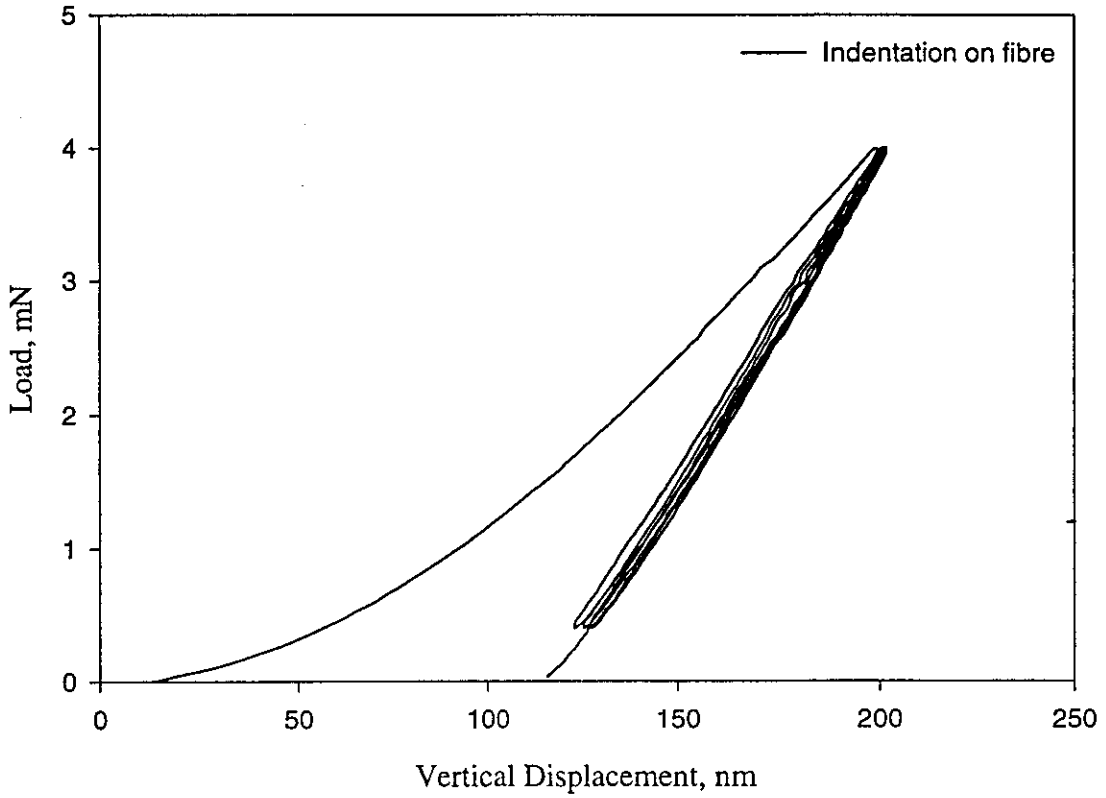
Indentation on fibre
Load, mN
Vertical Displacement, nm
0
1
2
3
4
5
0
50
100
150
200
250

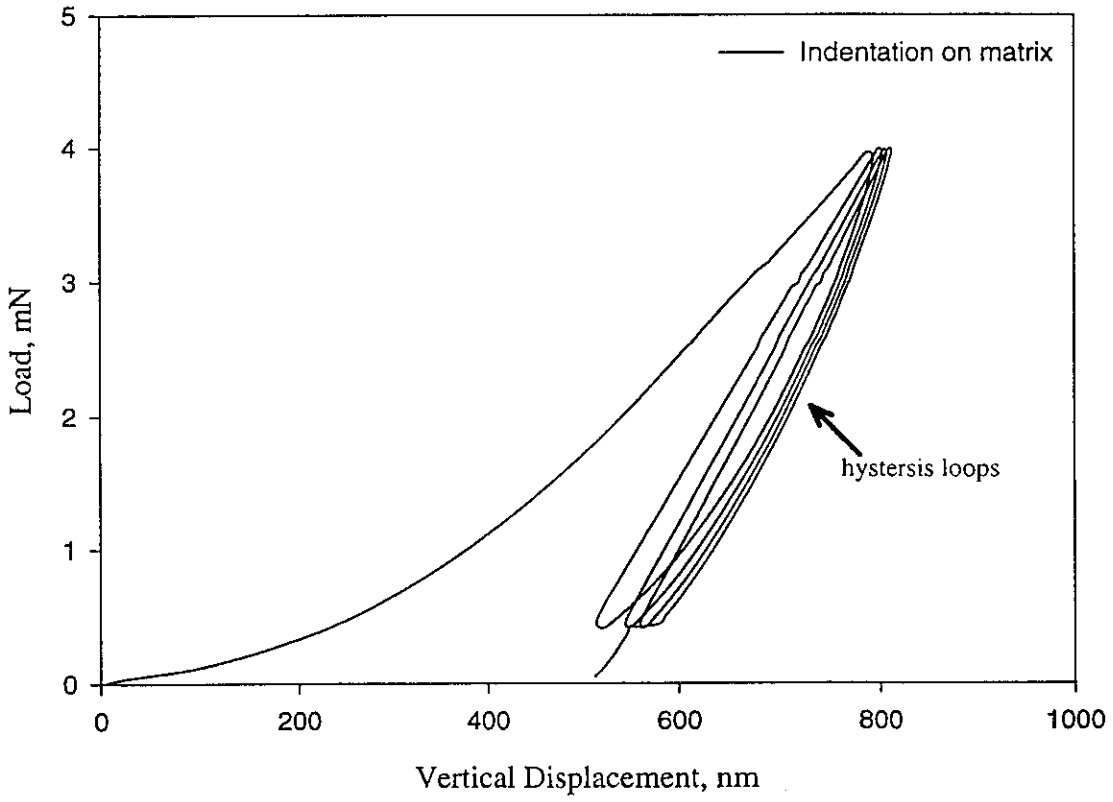
Indentation on matrix
hystersis loops
Load, mN
Vertical Displacement, nm
0
1
2
3
4
5
0
200
400
600
800
1000

Fig 5

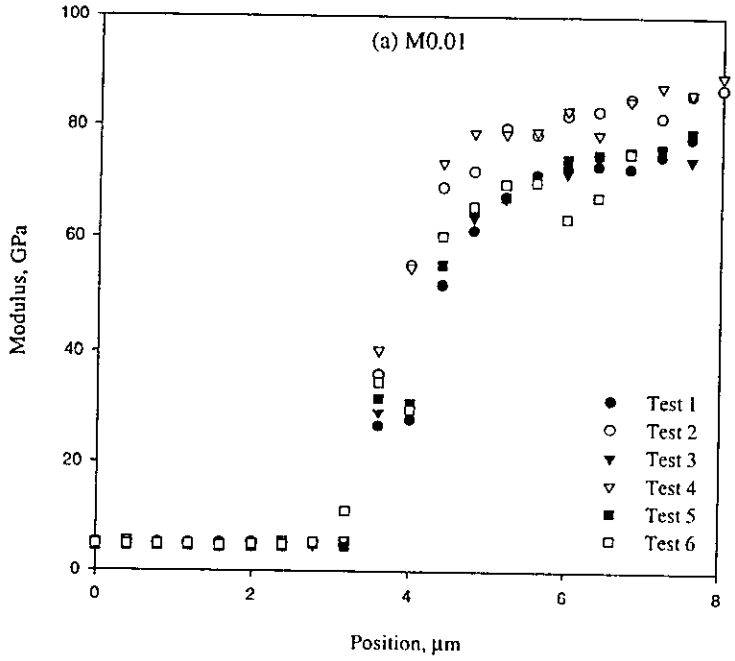
(a) M0.01
Modulus, GPa
Position, µm
Test 1
Test 2
Test 3
Test 4
Test 5
Test 6

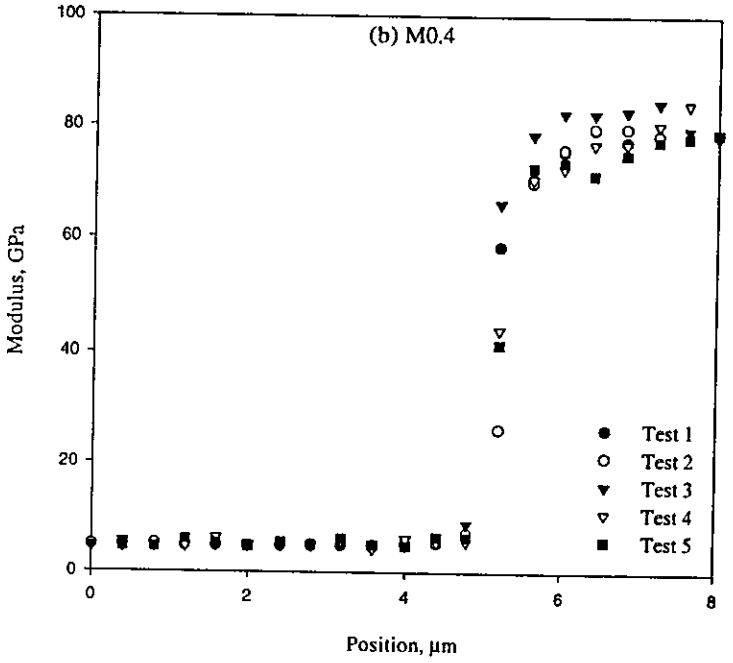
(b) M0.4
Modulus, GPa
Position, µm
Test 1
Test 2
Test 3
Test 4
Test 5

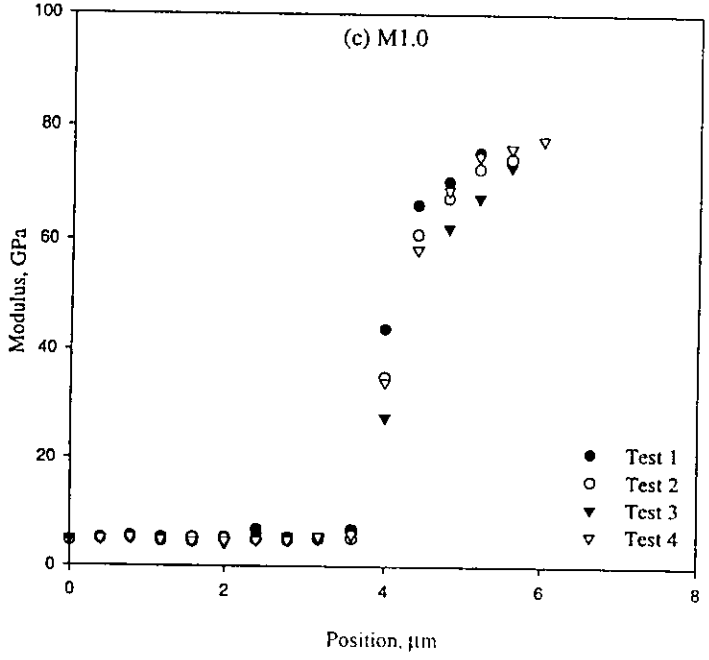
(c) M1.0
Modulus, GPa
Position, µm
Test 1
Test 2
Test 3
Test 4

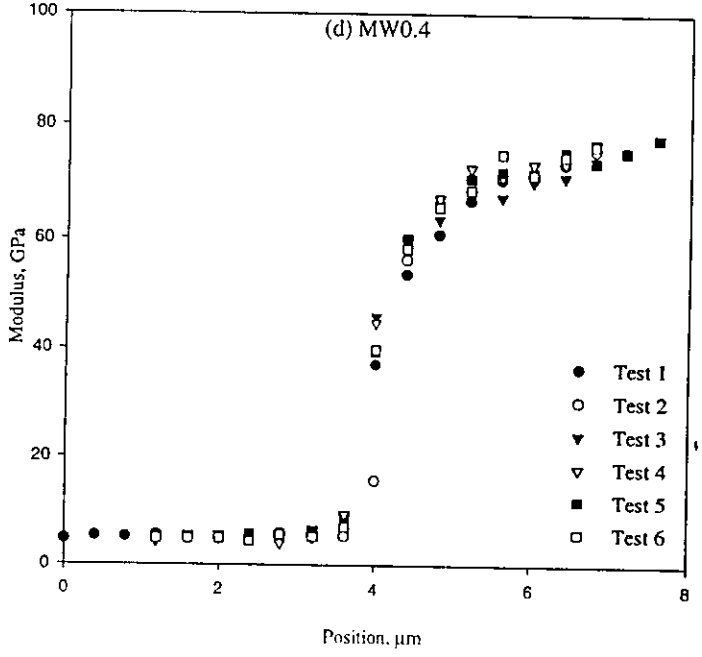
(d) MW0.4
Modulus, GPa
Position, µm
Test 1
Test 2
Test 3
Test 4
Test 5
Test 6

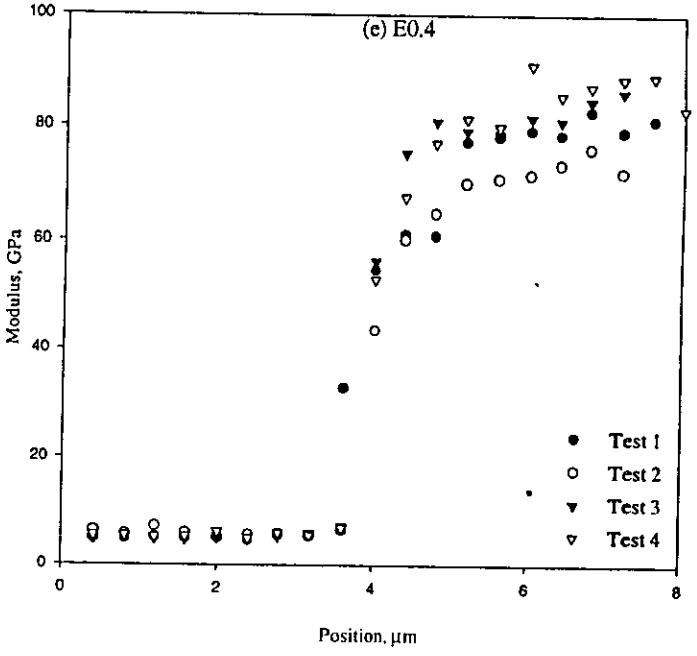
(e) E0.4
Modulus, GPa
Position, µm
Test 1
Test 2
Test 3
Test 4

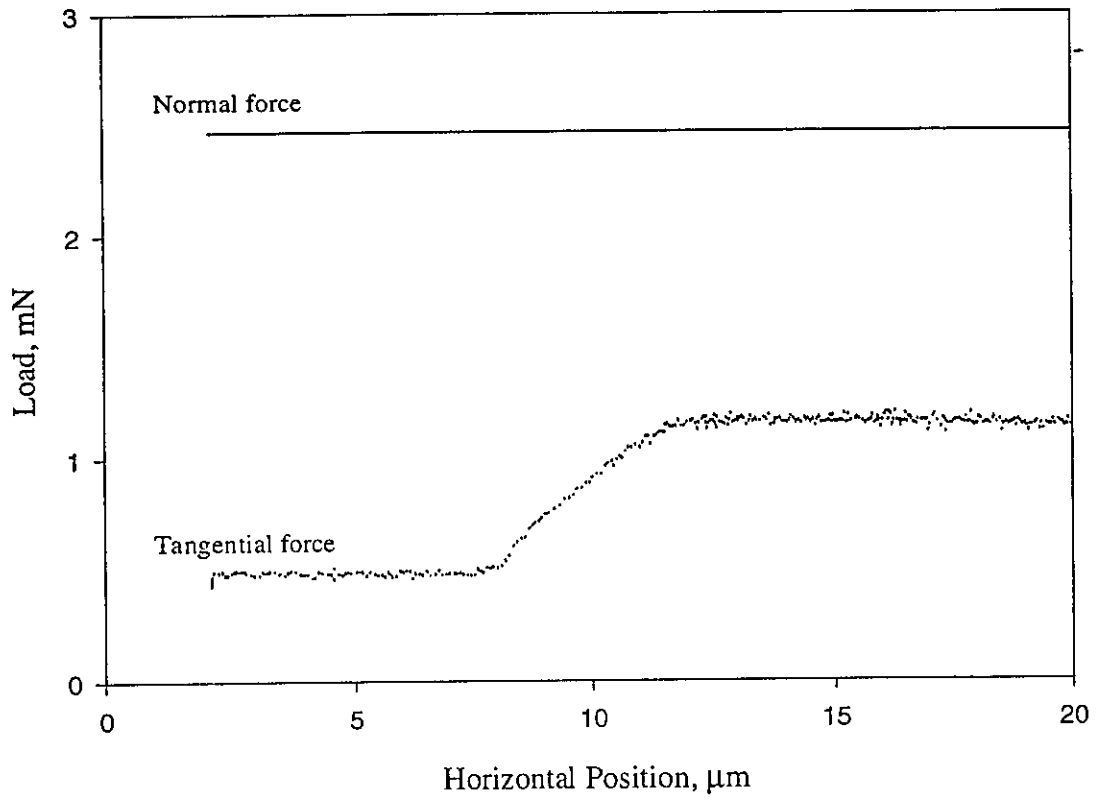
Normal force
Tangential force
Load, mN
Horizontal Position, µm
0
1
2
3
0
5
10
15
20

Fig 7

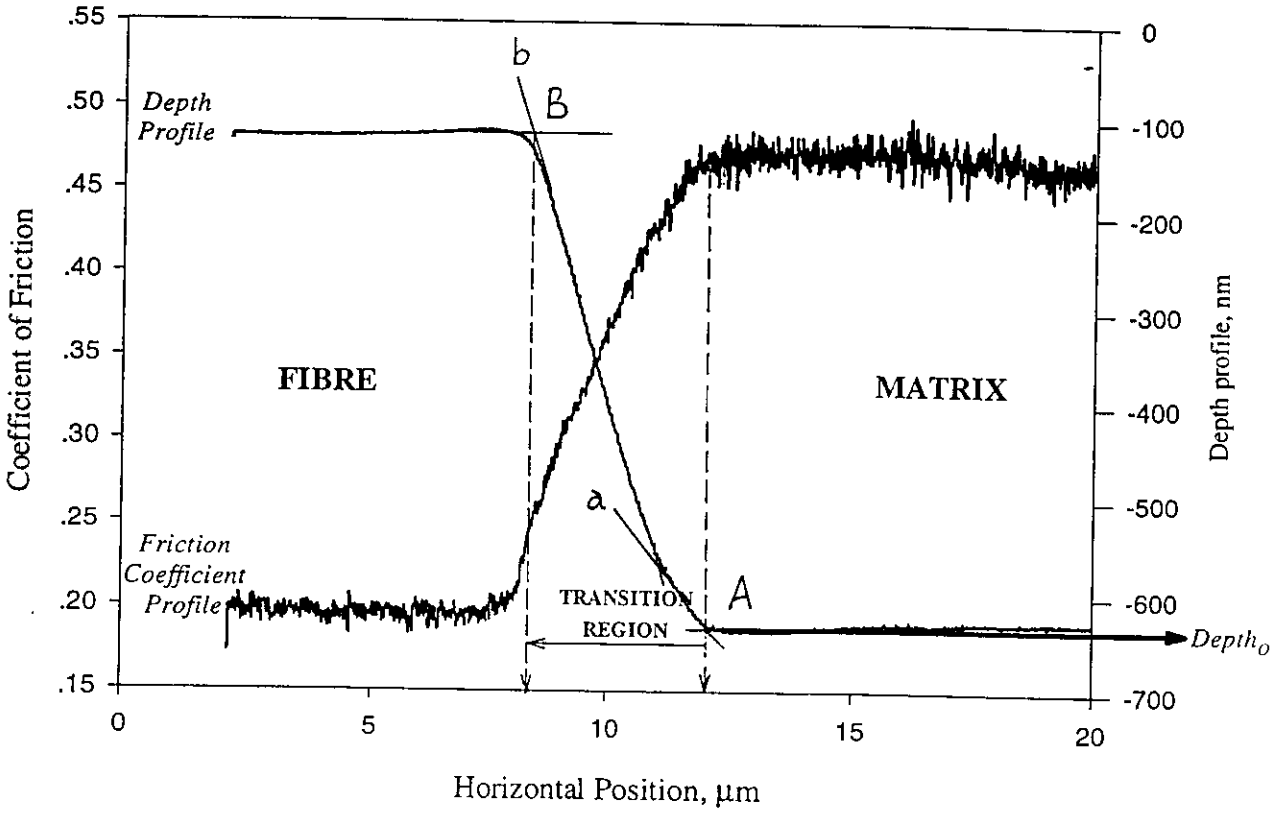
.55
.50
.45
.40
.35
.30
.25
.20
.15
Coefficient of Friction
0
-100
-200
-300
-400
-500
-600
-700
Depth profile, nm
Depth Profile
Friction Coefficient Profile
FIBRE
MATRIX
b
B
a
A
TRANSITION REGION
Depth$_o$
0
5
10
15
20
Horizontal Position, µm

Fig 8

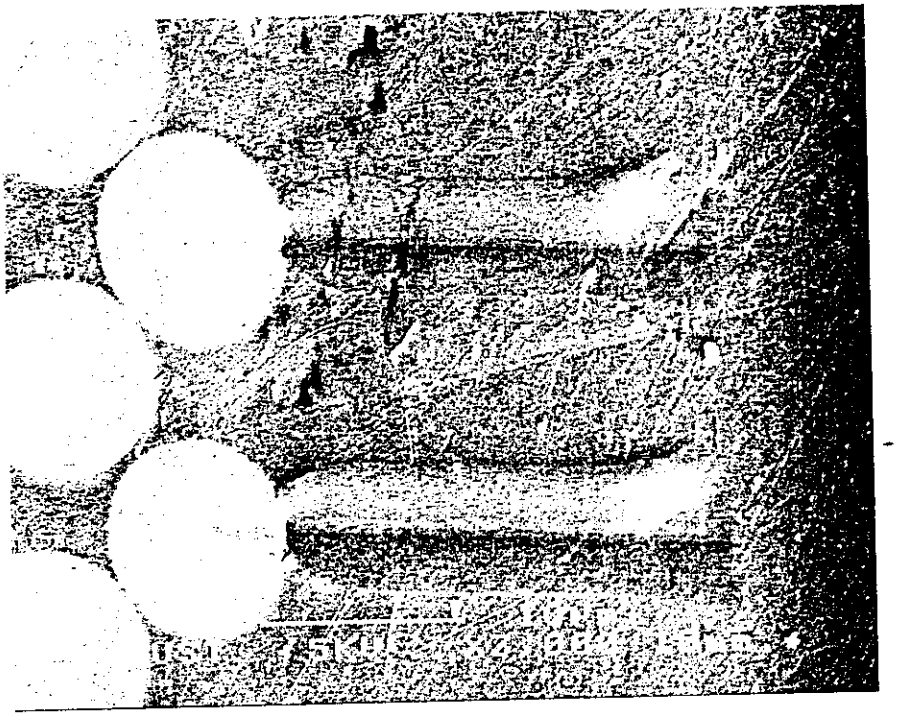

Fig 9

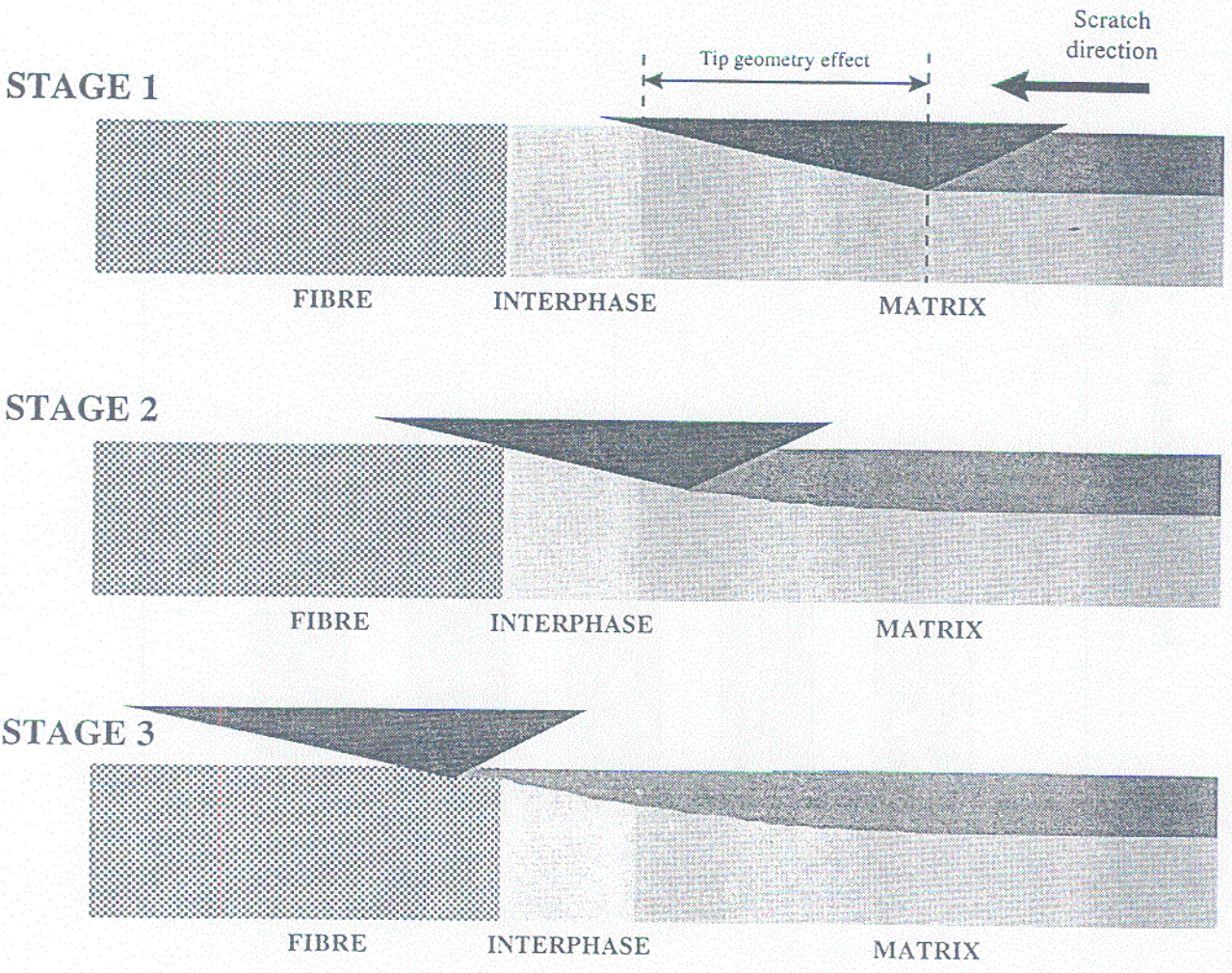
STAGE 1
Tip geometry effect
Scratch direction
FIBRE
INTERPHASE
MATRIX
STAGE 2
FIBRE
INTERPHASE
MATRIX
STAGE 3
FIBRE
INTERPHASE
MATRIX

Fig 10

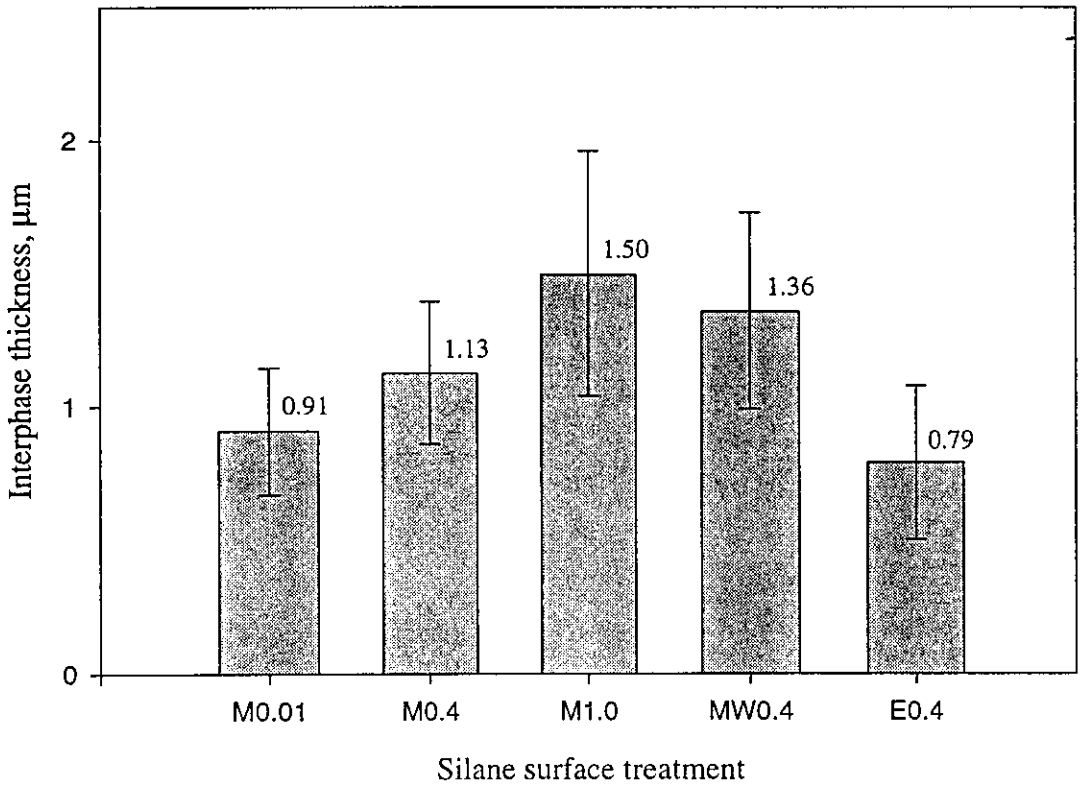
Interphase thickness, µm
2
1
0
0.91
1.13
1.50
1.36
0.79
M0.01
M0.4
M1.0
MW0.4
E0.4
Silane surface treatment

Fig 11

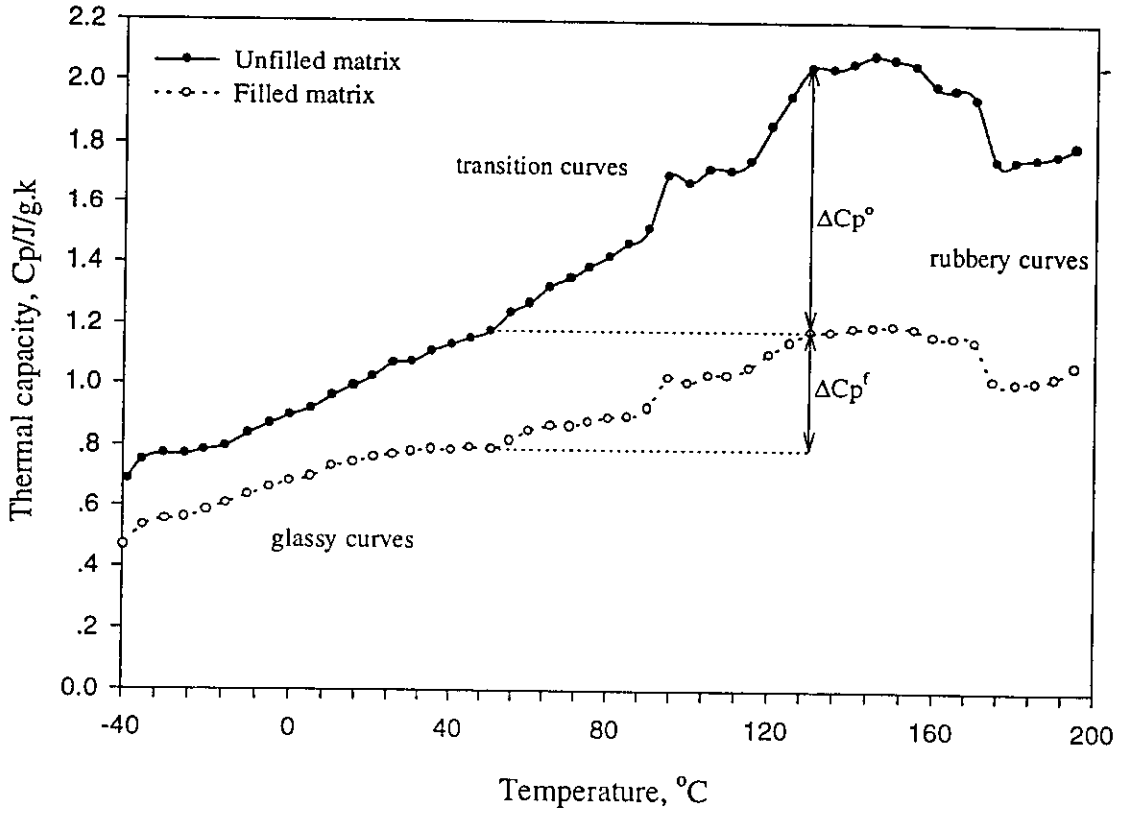
Unfilled matrix
Filled matrix
transition curves
rubbery curves
glassy curves
ΔCp°
ΔCp^f
Thermal capacity, Cp/J/g.k
Temperature, °C
2.2
2.0
1.8
1.6
1.4
1.2
1.0
.8
.6
.4
.2
0.0
-40
0
40
80
120
160
200

Fig 12

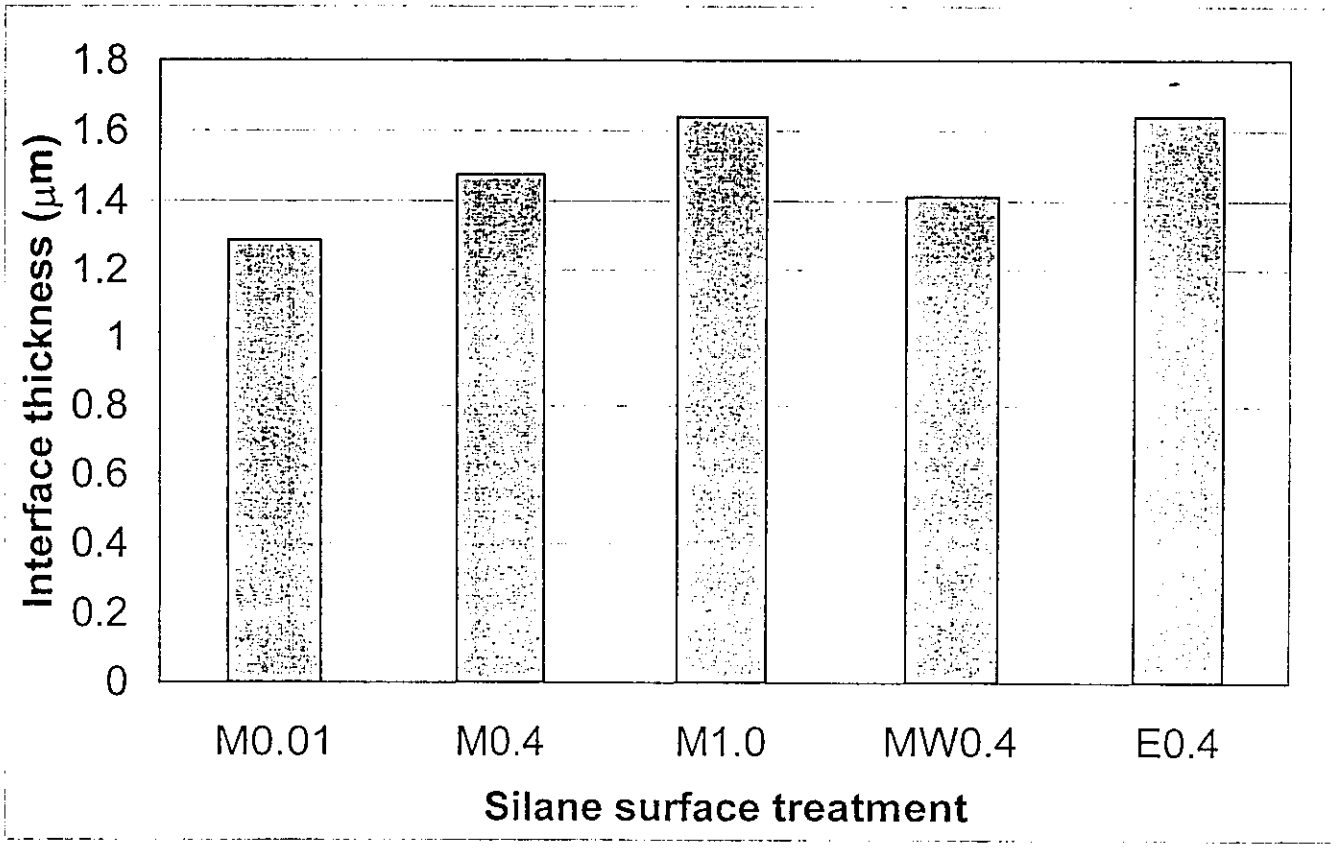
Interface thickness (μm)
1.8
1.6
1.4
1.2
1
0.8
0.6
0.4
0.2
0
M0.01
M0.4
M1.0
MW0.4
E0.4
Silane surface treatment

Fig 13